

PHOTOCHEMISTRY
AND MAGNETOCHEMISTRY

First-Principles Design and Preparation of Ag_3PO_4 Materials and Their Photocatalytic Properties

Chao Peng^a, Yunfeng Liu^a, Junhao Cui^a, Kun Luo^b, Yi Shen^{a,*}, and Xiaohui Li^{a,**}

^a Key Laboratory of Environment Functional Materials of Tangshan City, Hebei Provincial Key Laboratory of Inorganic Nonmetallic Materials, Industry Institute of Advanced Materials and College of Materials Science and Engineering, North China University of Science and Technology, Tangshan, Hebei, 063210 China

^b Center for High Pressure Science (CHIPS), State Key Laboratory of Metastable Materials Science and Technology, Yanshan University, Qinhuangdao, 066004 China

*e-mail: shenyi686@163.com

**e-mail: lixiaohui76543@163.com

Received August 7, 2020; revised November 3, 2020; accepted November 3, 2020

Abstract—The charge density, differential charge density, band structure, density of states and absorption spectra of cubic structure Ag_3PO_4 were calculated by Material Studio software. The best function for calculating the Ag_3PO_4 crystal model is PBE0 with a lattice constant of 6.004 Å. In Ag_3PO_4 crystal system, the force between O–Ag is weaker than that between O–P, which leads to the photo-corrosion of Ag_3PO_4 material. The forbidden band width of the Ag_3PO_4 crystal is 2.47 eV. The light absorption boundary is approximately 520 nm. At the same time, the cubic phase Ag_3PO_4 was successfully prepared. The light absorption boundary value of the Ag_3PO_4 sample measured by UV–Vis diffuse reflectance spectroscopy is about 520 nm, and the forbidden band width is 2.41 eV. The results obtained by means of photoluminescence spectroscopy, UV–Vis diffuse reflectance absorption spectroscopy and degradation of organic pollutants are consistent with theoretical calculations.

Keywords: first-principles, Ag_3PO_4 , photocatalytic, CASTEP

DOI: 10.1134/S0036024421130173

INTRODUCTION

When solving the Schrödinger equation of multi-particle system, the eigenfunction of Schrödinger equation is obtained by approximating the physical knowledge, such as basic physical law, density functional theory, quantum mechanics, etc., and the material is calculated according to the wave function of the system. The nature of this is what we call first-principles calculations [1–4]. It brings the dawn of a new material design in the true sense. Photocatalytic materials absorb sunlight and achieve the purpose of degrading organic pollutants by redox reaction with pollutants in the environment. It has shown excellent performance in environmental protection and clean energy, which will greatly benefit the development of the future society [5–8]. Therefore, the research and development of photocatalytic materials have received more and more attention [9–11]. The use of solar energy to control environmental pollution has become a hot research topic in the field of photocatalysis [12–15].

In 2011, Ye Jinhua's research group successfully applied silver phosphate to the photocatalytic direction, which is superior to other types of semiconductor photocatalysts in degrading organic pollutants and produc-

ing oxygen, such as titanium dioxide [16–20], zinc oxide, bismuth vanadate, carbon nitride, silver halide, and the like. The forbidden band width of Ag_3PO_4 is 2.43 eV, which determines that Ag_3PO_4 can absorb light in the ultraviolet-visible band of less than 530 nm, and the visible light response range is large. The valence band potential of Ag_3PO_4 is 2.88 eV. The rate of hydrogen production by Ag_3PO_4 decomposed by Ye et al. is 8.8 and 2.6 times that of WO_3 and BiVO_4 , respectively. The degradation rate of Ag_3PO_4 to methylene blue is several times faster than the reported BiVO_4 . The photocatalyst is modified with a nano metal, and in the region where the nano metal contacts the semiconductor, electrons are transferred from the inside of the photocatalytic material to the metal to form a Schottky barrier [21–24]. The photogenerated electrons are prevented from recombining with the holes, and the photocatalytic activity of Ag_3PO_4 is improved.

When silver phosphate is exposed to air, it is easily oxidized. During long-term contact with air, silver phosphate produces photochemical corrosion [25, 26]. And the generated silver element will cover the surface of the silver phosphate particles, reduce the

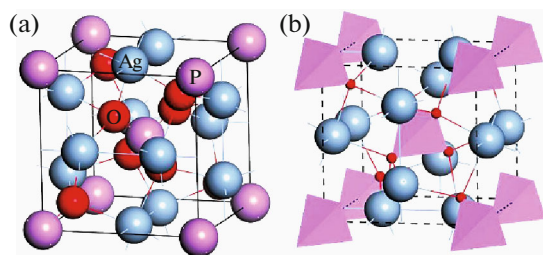


Fig. 1. Cellular model of silver phosphate.

utilization of light by the silver phosphate, and greatly reduce the activity of the silver phosphate. In addition, the process of preparing silver phosphate requires a large amount of Ag consumption, which is expensive and limits its large-scale application. The nano metal particles are loaded on the surface of the semiconductor photocatalytic to generate a ionic resonance effect, which can cause the absorption spectrum of the composite photocatalyst to red-shift and allow the photocatalyst to absorb visible light [27–30]. This plasmon resonance effect of noble metal nanoparticles allows the nanoparticles to exhibit a strong visible light absorption effect in the visible light region and thereby improve the photocatalytic efficiency of the semiconductor.

Material Studio is a material calculation software based on first-principles principle. By establishing the unit cell of the material, the electronic structure, optical properties, surface properties, mechanical properties, etc. of the material can be directly calculated after parameter setting [31–33]. In order to further study the catalytic mechanism of silver phosphate photocatalytic materials, some researchers have used the CASTEP module in Material Studio to study the multi-faceted properties of silver phosphate and deepen the understanding of the photocatalytic reaction mechanism of silver phosphate. It will play a positive guiding role in the development of silver phosphate photocatalyst.

Based on the above conditions, Ag_3PO_4 and nano-metal modified Ag_3PO_4 model were established by CASTEP module in Materials Studio. The crystal cell structure of Ag_3PO_4 and nano-metal modified Ag_3PO_4 were calculated. The mechanism of nano metal modified photocatalytic materials was analyzed. Nano-modified Ag_3PO_4 photocatalytic materials were prepared by experiments and verified by calculation results [34–38].

CALCULATIONS

In this paper, the CASTEP module in the Material Studio software is used to calculate the properties of the system. The CASTEP module mainly uses the density functional theory and the plane wave pseudo-potential to calculate the solid material theoretically. The electron wave function is extended by the plane wave basis set, the number of base groups is deter-

mined by the cutoff energy, and the cutoff energy is set to 500 eV. Because the LDA and GGA series of functions are not very accurate in calculating the semiconductor band structure and the density of electronic states. So this paper selects the function PBE0 for the calculation of the properties of silver phosphate materials. The description of the electrons is consistent with the actual amount of charge, the number of plane wave base groups is small, and the amount of computer computation is small. In the established silver phosphate model, $4d^{10}5s^1$ of Ag, $3s^23p^3$ of P, and $2s^22p^4$ of O are regarded as valence states. Silver phosphate is a bulk material, so the K -point of the Brillouin zone where silver phosphate is set in the geometrical optimization is $4 \times 4 \times 4$. Since the local density approximation is only applicable to systems with slow electron density changes, the wide-area density approximation is used when studying the silver phosphate model.

The crystal model of Ag_3PO_4 is a body-centered cubic structure with a space group of $P\bar{4}3n$. The basic structural units are PO_4 tetrahedron and $\text{Ag}-\text{PO}_4$ tetrahedral structure. The P atom forms a PO_4 tetrahedron with four adjacent oxygen atoms. Ag atoms are distributed around the PO_4 tetrahedron. From another point of view, the Ag_3PO_4 crystal model can also be regarded as a PO_4^- tetrahedron forming a body-centered cubic lattice, and Ag atoms are distributed at the symmetry points of adjacent PO_4^- tetrahedra. The fractional coordinates of each atom in the Ag_3PO_4 crystal are Ag (0.25, 0, 0.5), P (0, 0, 0), O (0.148, 0.148, 0.148). The lattice constant of Ag_3PO_4 is theoretically 6.004 Å. The unit cell model of Ag_3PO_4 is shown in Fig. 1: where (a) is the model of the club model and (b) is the model of the polyhedron model.

MATERIALS AND METHODS

Preparation of Silver Phosphate by Coprecipitation

Weigh 0.02 mol of AgNO_3 and mix it with 50 mL of distilled water, and stir until dissolved. Dilute 5 times diluted ammonia water, continue to drop after the brown precipitate appears, stop the addition when the precipitate just disappears. Dilute 5 times diluted nitric acid into the configured silver ammonia solution until the pH of the silver ammonia solution stop at pH 8. Weigh 0.03 mol KH_2PO_4 and mix with 50 mL of distilled water, stir to dissolve, form KH_2PO_4 solution, and add KH_2PO_4 solution to the silver ammonia solution dropwise, stir for 30 min. After stirring, let stand at room temperature for 15 min. Then, it was washed three times with deionized water and absolute ethanol, and dried in a vacuum oven at 70°C for 40 min.

Characterization

The phase of the sample was analyzed with a Ultima IV X-ray powder diffraction (XRD) instrument ($\text{CuK}\alpha$,

$\lambda = 0.15418$ nm, operating voltage 40 kV, current 40 mA, scanning range $\sim 10^\circ$ – 80°). Hitachi S4800 Scanning Electron Microscope (SEM) was used to determine the morphology and microstructure of the photocatalyst sample. The UV–Vis diffuse absorption spectrum of the sample was measured on a Shimadzu 2550 UV–Vis spectrometer with a scanning range of 200 to 700 nm. The F-4500 type fluorescence spectrometer was used to measure the photoluminescence spectrum of the sample, and the scanning range was ~ 200 – 700 nm.

Photocatalytic Activity Evaluation

First, pour 50 mL of RhB simulated pollutant solution with a concentration of 5 mg L^{-1} into the reactor, then add 50 mg of catalyst. Before the visible light irradiation, perform first a dark reaction for 30 min (only the reactor stirring function is turned on), and the rotation speed is 500 rpm to ensure that the adsorption/desorption equilibrium is established. The white light-emitting diode (wLED) equipped with the PCX-50B multi-channel photocatalytic reaction system (Beijing Pofilai Technology Co., Ltd., Beijing, China) is used as the light source for light. The speed of the reactor is 500 rpm, and the brightness of the wLED lamp during the reaction is 0.7 A. Turn on the light source to carry out the photocatalytic reaction. Pipette 2.0 mL of the reaction solution at regular intervals. After centrifugal separation, take the supernatant for UV–Vis spectrum analysis. The scanning range is ~ 200 – 800 nm, and the RhB detection is selected at the characteristic absorption peak of 553 nm in the visible region. The relationship between absorbance and concentration is following the Beer–Lambert law, and the degradation rate $D = (A_0 - A)/C_0 \times 100\%$ is obtained according to the change of the absorbance value of the sample. Among them, A_0 and A are the initial absorbance value of the sample and the absorbance value after degradation, respectively. With the difference of reaction time, according to the aforementioned formula, the degradation status and degradation rate of rhodamine B by the catalyst can be obtained.

RESULTS AND DISCUSSION

Maliken Layout Number and Chemical Bond Analysis

Studies have shown that the photocorrosion of Ag_3PO_4 is related to the bond energy between atoms. In order to clarify the distribution of charge in Ag_3PO_4 crystal and the bonding state between atoms, the Mulliken charge, the bond population and the chemical bond length of the Ag_3PO_4 crystal were calculated by the plane wave pseudopotential method. The calculation results are shown in Tables 1 and 2, respectively. The Mulliken charge distribution can quantitatively analyze the distribution of charge between atoms in the system. The number of bond populations can be

Table 1. Million charge (q) of key atoms

Model	Atom	q
Ag_3PO_4 crystal	O	−0.87
	P	2.09
	Ag	0.47

Table 2. Key layout of key atoms

Model	Bond	Population	Length, Å
Ag_3PO_4 crystal	O–P	0.59	1.57560
	O–Ag	0.14	2.37389
	O–O	−0.11	2.49389

seen in the type of bond formed by the atom. The strength of the interaction between atoms is characterized by the length of the chemical bond.

It can be seen from Table 1 that in the Ag_3PO_4 crystal system, the O atom is negatively charged, and each O atom finally obtains 0.87 electrons, while the Ag and P atoms lose electrons with positive charge, and the Ag atom loses 0.47 electrons. The P atom loses 2.09 electrons, and it can be clearly seen that the number of electrons lost by the P atom is much larger than the number of electrons lost by the Ag atom. It can be seen from Table 2 that the O–P bond length (1.57560 Å) is smaller than the O–Ag bond length (2.37389 Å), indicating that the interaction force between O–P is greater than the interaction force between O–Ag. We can judge the bonding of atoms by the number of bond populations. From Table 2, we can conclude that the O–P bond is a covalent bond and the O–Ag bond is an ionic bond. The negative value of the O–O bond indicates that the distance between the O atoms is far and the interaction is weak. It can be inferred from Tables 1 and 2 that there is a certain correlation between the O–P bond in the Ag_3PO_4 crystal and the electron-loss number of the O–Ag bond and the P atom being much larger than the electron loss number of the Ag atom. However, the weak interaction between O–Ag makes the metastable Ag ions easy to get electrons to be reduced to Ag and lose the photocatalytic effect, resulting in the photocorrosion performance of Ag_3PO_4 material.

Charge Density and Differential Charge Density Analysis

In order to visually describe the bonding form between atoms in the Ag_3PO_4 crystal, the charge density distribution map and the charge density difference map of all the atoms in the Ag_3PO_4 crystal were calculated, as shown in Figs. 2 and 3, respectively.

Figure 2 shows the distribution of charge density around the three atoms Ag, P, and O in the Ag_3PO_4 crystal. It can be clearly seen from Fig. 10 that the

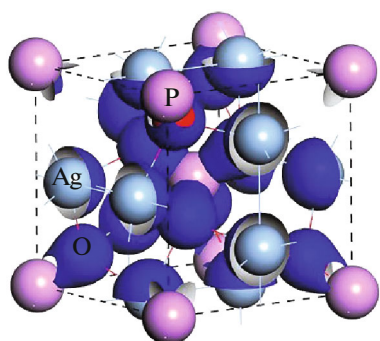


Fig. 2. Differential charge density of silver phosphate.

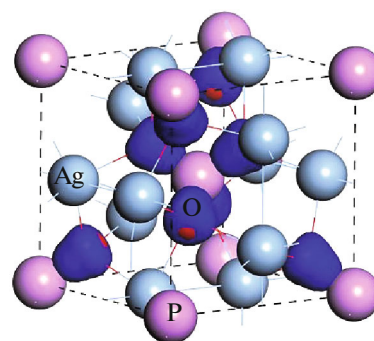


Fig. 3. Differential charge density map of silver phosphate.

electron cloud of the P atom partially overlaps with the electron cloud of the O atom and Ag. The electron cloud of the atom and the electron cloud of the O atom hardly overlap, which means that the force between the P-bonds is much higher than the force between the Ag–O bonds. This is consistent with the calculated bond population and Millikan charge properties. The overlapping electron clouds illustrate the interaction between atoms. Ag^+ which has lost electrons is in an unstable state in Ag_3PO_4 crystal, and is easily combined with electrons in photo-generated electron-hole pairs to be reduced into silver simple substance during photocatalysis. The occurrence of this situation destroys the original crystal structure of silver phosphate, which causes the material to slowly deteriorate and lose the photocatalytic performance.

The differential charge density map can show the charge density difference around each atom before and after bonding, that is, the charge transfer of each atom in the crystal. It can be seen from Fig. 3 that the charge density around the Ag atom is almost zero. This shows that the extremely weak interaction force between Ag^+ and PO_4^- is consistent with the above calculation results. Furthermore, it is obvious from Fig. 3 that the charge density is mostly concentrated around the O atom. There is charge transfer between O atom and P atom, and the interaction between the two is significantly higher than that between O atom and Ag atom. According to the density of states analysis, the hybridization between the S and P orbitals of O atom and P atom makes the interaction force between O atom and P atom strong in the form of covalent bond. The high charge density around O also increases the orbital hybridization degree of O atom and P atom, and increases the electron transfer and transition degree, making Ag_3PO_4 crystal have higher photocatalytic activity.

Analysis of Energy Band Structure and Density of States

Ag_3PO_4 as a semiconductor photocatalytic material, its photocatalytic performance is closely related to the forbidden band width. The forbidden band width directly determines the absorption range of the semiconductor photocatalytic material, which fundamen-

tally determines the photocatalytic activity of the semiconductor photocatalytic material. Generally, the forbidden band width of the material is underestimated when the forbidden band width is calculated by the local density approximation in the density functional theory. In order to accurately calculate the forbidden band width of Ag_3PO_4 semiconductor material, the forbidden band width of Ag_3PO_4 semiconductor material is calculated by hybrid functional PBE0.

Figure 4 is an energy band structure diagram of Ag_3PO_4 semiconductor material calculated using PBE0 function. The dotted line at energy 0 in the figure is the Fermi level. It can be seen from Fig. 4 that the bottom end of the conduction band of the Ag_3PO_4 crystal is located at the G point of the Brillouin zone, and the value is 2.47 eV. The top of the valence band is located at the M point of the Brillouin zone, and the value is 0.04 eV. The top of the G-point price band is 0.00 eV. Therefore, Ag_3PO_4 crystal is an indirect band-gap semiconductor material. This will greatly reduce the recombination rate of photo-generated electron-hole pairs and improve the photocatalytic performance. The calculated forbidden band width of Ag_3PO_4 crystal is 2.47 eV. The theoretical calculation results are basically consistent with the experimental results (2.43 eV), which shows that the first principle calculation results are accurate and reliable. It can also be seen from the figure that the electrons at the bottom of the conduction band have strong dispersibility, which indicates that the effective mass of photogenerated electrons in the conduction band portion is small,

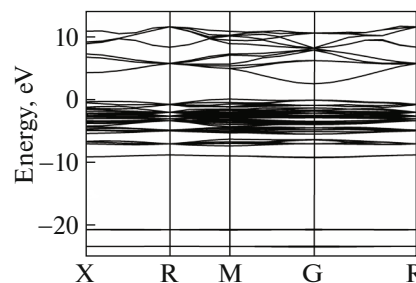


Fig. 4. Energy band structure diagram of Ag_3PO_4 .

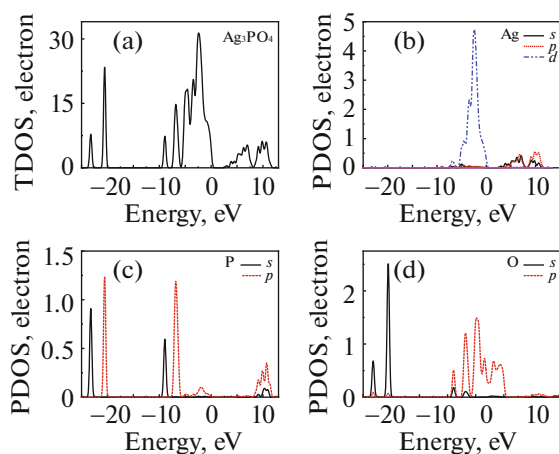


Fig. 5. State density map of Ag_3PO_4 .

which is conducive to the transfer of electrons and further helps to improve the photocatalytic activity of Ag_3PO_4 semiconductor photocatalytic material.

In order to further explain the electronic structure of Ag_3PO_4 crystal, we have calculated the total density of states of Ag_3PO_4 crystal and the fractional density of states of each atom in the crystal by the same method. The calculation results are shown in Fig. 5. For a physical system, the energy distribution determines the state of the system or the performance of the material. The density of states actually corresponds to the energy distribution. It can be seen from the figure that the Fermi level of Ag_3PO_4 crystal is in the region where the density of states is equal to zero, which indicates that Ag_3PO_4 crystal is a semiconductor material.

At the total density of states values of -23 , -20 eV and from about -10 to -5 eV, it can be seen from the density of states diagram that the valence state is mainly formed by hybridization of the S and P orbitals of O and P respectively. The top of the valence band at the from about -5 to 0 eV range is mainly provided by the O $2p$ and Ag $4d$ orbitals, and a small amount of P $3p$ orbitals are also dispersed in this range. The dispersion widths of the O $2p$ and Ag $4d$ orbitals are relatively wide, which indicates that electrons have a small effective mass, which will help electrons transition from valence band to conduction band. Among them, the Ag $4d$ orbit accounts for the main part, which is a big spike and there is no orbital splitting phenomenon. This indicates that the orbit is highly localized. The right side of the Fermi level is the conduction band part, which is mainly provided by the Ag $5s$ and Ag $5p$ orbitals. These two orbitals have a wide distribution range, which shows that the electron transition from valence band to conduction band part has strong non-locality, and on the one hand, it is conducive to the electron moving from the inside of the material to the surface for photocatalytic action. On the other hand, the probability of recombination of electrons and

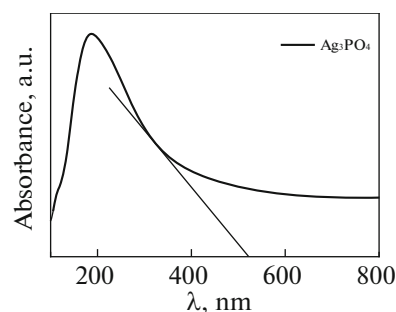


Fig. 6. Absorption spectrum of Ag_3PO_4 .

metastable Ag^+ is increased, resulting in photocorrosion.

Optical Property Analysis

Ag_3PO_4 photocatalysis material can efficiently degrade organic pollutants represented by rhodamine B in water under visible light irradiation. In order to explore the relationship between the microstructure and optical properties of Ag_3PO_4 photocatalyst. In this paper, the optical absorption coefficient of Ag_3PO_4 photocatalytic material was calculated by density functional theory, the correlation between electronic structure and optical absorption characteristics was explored, and the catalytic mechanism of Ag_3PO_4 photocatalytic material was further studied. As the hybrid functional PBE0 is used to calculate the band structure of Ag_3PO_4 , the obtained band gap of Ag_3PO_4 crystal has a small error with the experimental value, so the same calculation method is still used to calculate the light absorption coefficient.

Figure 6 is a graph showing the absorption spectrum of Ag_3PO_4 crystal calculated by PBE0 hybrid function, which Intuitive display of the absorption of different wavelengths of light by Ag_3PO_4 . It can be seen from the figure that Ag_3PO_4 crystal has absorption intensity in both the ultraviolet region and the visible region. In particular, Ag_3PO_4 crystals have a large absorption of light in the visible range. It was confirmed that Ag_3PO_4 is a visible light responsive photocatalytic material. The light absorption boundary value of Ag_3PO_4 crystal is about 520 nm. Combined with the state density map of the crystal, it can be seen that the absorption of light by Ag_3PO_4 crystal mainly provides energy for the transition of electrons in the O $2p$ orbit to the Ag $5s$ orbit.

Preparation of Ag_3PO_4

In order to verify the authenticity and accuracy of the calculation results, cubic Ag_3PO_4 samples were prepared by coprecipitation method in this chapter. The samples were tested by XRD and the analysis results are as follows:

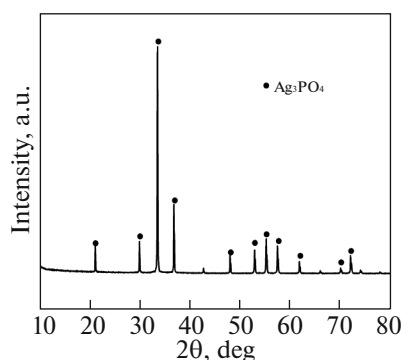


Fig. 7. XRD pattern of silver phosphate prepared by coprecipitation method.

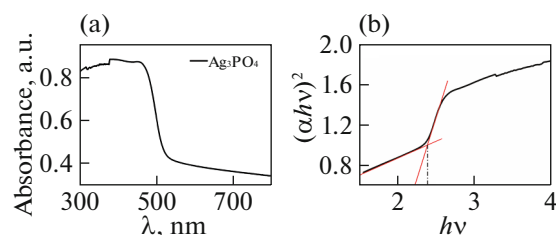


Fig. 9. The UV-Vis DRS and the E_g images of Ag_3PO_4 .

Figure 7 is an XRD pattern of the prepared Ag_3PO_4 sample. through observation, diffraction peaks appear at diffraction angles $2\theta = 20.86^\circ, 29.74^\circ, 33.30^\circ, 36.64^\circ, 42.40^\circ, 47.78^\circ, 52.78^\circ, 55.44^\circ, 57.68^\circ,$ and 61.80° , corresponding to (110), (200), (210), (220), (310), (310), (222), (320), (321) crystal planes of Ag_3PO_4 . Corresponding to the diffraction peak of Ag_3PO_4 (JCPDS no. 06-0505) crystal with body-centered cubic structure, the intensity of diffraction peak is relatively high, indicating good crystallization performance. It can be explained that the cubic Ag_3PO_4 needed by the experiment was successfully prepared. Subsequent test results can be used to compare with theoretical calculation results.

In order to further clarify the cubic structure of Ag_3PO_4 samples, the samples were characterized by SEM. Figure 8 is the morphology characterization result of Ag_3PO_4 sample prepared by coprecipitation method, showing that the morphology of Ag_3PO_4 prepared by experiment is cubic phase. This indicates that cubic Ag_3PO_4 was successfully prepared by the coprecipitation method. But at the same time, we can also observe that the particle size of Ag_3PO_4 prepared in this experiment is different, the larger crystal grain is about 500 nm, while the smaller is only a few tens of nm, which also shows from the side that the growth of Ag_3PO_4 crystal grain is random in the process of preparing Ag_3PO_4 by coprecipitation. The size of Ag_3PO_4 particles is not uniform, but all are cubic crystals, which will not affect the photocatalytic performance results measured by experiments.

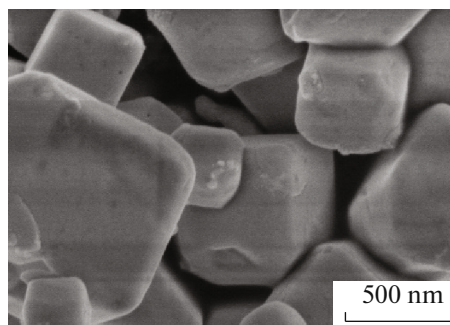


Fig. 8. SEM map of Ag_3PO_4 sample.

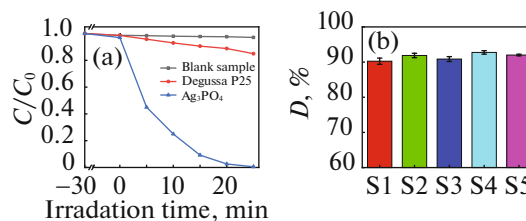


Fig. 10. (a) Degradation of rhodamine B under visible light irradiation; (b) in five parallel experiments of Ag_3PO_4 photocatalytic degradation, the degradation rate of rhodamine B at 15 min.

From the above theoretical calculation results, it can be seen from the energy band structure that the forbidden band width (E_g) of Ag_3PO_4 is 2.47 eV, and the optical absorption range of Ag_3PO_4 is calculated to be around 520 nm. Figure 9a is the light absorptivity of Ag_3PO_4 sample measured by UV-Vis diffuse reflectance spectroscopy. It can be seen that the maximum light absorption boundary value of Ag_3PO_4 sample is also around 520 nm, which is consistent with the theoretical calculated light absorption boundary value of Ag_3PO_4 . Figure 9b is a Tauc plot of the Ag_3PO_4 sample with the abscissa ($h\nu$) and the ordinate $(\alpha h\nu)^2$. As can be seen from Fig. 9b, the band gap of the Ag_3PO_4 sample is 2.41 eV. Ag_3PO_4 can absorb light in the visible light range, proving that Ag_3PO_4 is a visible light responsive photocatalyst. The test results of forbidden band width are consistent with the above theoretical calculation results.

Researchers have long used the effect of photocatalytic degradation of organic pollutants to judge the photocatalytic effect of photocatalysts. In order to detect the photocatalytic performance of Ag_3PO_4 with cubic phase, the photocatalytic performance of rhodamine B as organic pollutant was tested in this experiment. In Fig. 10a, it can be seen that the absorbance of rhodamine B in the blank sample did not change significantly, which ruled out the possibility of rhodamine B self-degradation. The degradation rate of rhodamine B by Ag_3PO_4 can reach about 90% within 15 min and about 99% within 25 min. Under the same conditions, the degradation rate of

rhodamine B by Degussa P25 is only about 10% at 25 min. This shows that the Ag_3PO_4 prepared in this experiment has very excellent photocatalytic activity. In Fig. 10b, it can be seen that the degradation rate of rhodamine B by Ag_3PO_4 at 15 min in five parallel experiments is about 90%, which can indicate that the photocatalytic performance of Ag_3PO_4 prepared in each experiment is basically the same.

CONCLUSIONS

In this paper, the crystal model of cubic structure Ag_3PO_4 was established by using Material Studio software. The properties of band structure, density of states, differential charge density and absorption spectrum were calculated by CASTEP module. In order to verify the calculation results, cubic structure of Ag_3PO_4 was prepared and its properties were characterized by various testing methods. The main conclusions are.

(1) It can be seen from the calculation results, in the Ag_3PO_4 crystal system, the electron cloud of the P atom in the Ag_3PO_4 crystal partially overlaps with the electron cloud of the O atom, and the electron cloud of the Ag atom and the electron cloud of the O atom hardly overlap, which indicates that the bond strength between the P–O bonds is much higher than that of the Ag–O. The bond between the O keys is strong. The charge density around the Ag atoms in the differential charge density map is almost zero. This shows a very weak interaction between Ag^+ and PO_4^- , and the charge density is mostly concentrated around the O atom. The interaction between the O atom and the P atom is significantly higher than the interaction between the O atom and the Ag atom. This is also the reason why Ag–O bond in Ag_3PO_4 is easy to break and photocorrosion occurs.

(2) The forbidden band width of the Ag_3PO_4 crystal is 2.47 eV. The theoretical calculation results are basically consistent with the experimental results (2.43 eV). The conduction band bottom of the Ag_3PO_4 crystal is mainly provided by the *s* orbital of the Ag and the *p* orbital, in which the *s* orbit dominates. The light absorption boundary of the Ag_3PO_4 crystal is approximately 520 nm.

(3) The Ag_3PO_4 sample prepared by the coprecipitation method completely degraded Rhodamine B in the solution within 25 min. The XRD pattern showed that the Ag_3PO_4 prepared by the experiment was a body-centered cubic structure of Ag_3PO_4 (JCPDS no. 06-0505). The SEM image shows the morphology of the experimentally obtained Ag_3PO_4 as a cubic phase. The light absorption boundary value of the Ag_3PO_4 sample measured by UV–Vis diffuse reflectance spectroscopy is around 520 nm. The above experimental results are consistent with the theoretical calculation results.

FUNDING

This work was funded by the National Natural Science Foundation of China (grant nos. 51772099, 51572069, 51872091), Scientific and Technological Research Projects of Colleges and Universities in Hebei Province (QN2019049).

DATA

All data generated or analyzed during this study are included in this article.

CONFLICT OF INTEREST

Top author's name and other co-authors have no conflict of interest.

REFERENCES

1. X. Chen, S. Shen, L. Guo, and S. S. Mao, *Chem. Rev.* **110**, 6503 (2010).
2. K. Woan, G. Pyrgiotakis, and W. Sigmund, *Adv. Mater.* **21**, 2233 (2009).
3. S. Sakthivel, B. Neppolian, M. V. Shankar, B. Arabin-doo, M. Palanichamy, and V. Murugesan, *Sol. Energy Mater. Sol. Cells* **77**, 65 (2003).
4. A. Wold, *Chem. Mater.* **5**, 280 (1993).
5. S. K. Zheng, T. M. Wang, and C. Wang, *J. Mater. Sci. Lett.* **21**, 1721 (2002).
6. H. G. Kim, P. H. Borse, W. Choi, and J. S. Lee, *Angew. Chem., Int. Ed.* **44**, 4585 (2005).
7. J. Wang, D. N. Tafen, J. P. Lewis, Z. Hong, A. Manivannan, M. Zhi, et al., *J. Am. Chem. Soc.* **131**, 12290 (2009).
8. A. di Paola, E. García-López, G. Marci, and L. Palmisano, *J. Hazard. Mater.* **211**, 3 (2012).
9. K. Striegler, *Modified Graphitic Carbon Nitrides for Photocatalytic Hydrogen Evolution from Water: Copolymers, Sensitizers, and Nanoparticles* (Springer, New York, 2015).
10. Y. Yoshida, M. Matsuoka, S. C. Moon, H. Mametsuka, E. Suzuki, and M. Anpo, *Res. Chem. Intermed.* **26**, 567 (2000).
11. T. An, H. Zhao, and P. K. Wong, *Advances in Photocatalytic Disinfection* (Springer, Berlin, 2017).
12. K. L. Zhang, C. M. Liu, F. Q. Huang, C. Zheng, and W. D. Wang, *Appl. Catal. B: Environ.* **68**, 125 (2006).
13. J. Lin, C. Y. Jimmy, D. Lo, and S. K. Lam, *J. Catal.* **183**, 368 (1999).
14. C. C. Wang, J. R. Li, X. L. Lv, Y. Q. Zhang, and G. Guo, *Energy Environ. Sci.* **7**, 2831 (2014).
15. H. Irie, Y. Watanabe, and K. Hashimoto, *J. Phys. Chem. B* **107**, 5483 (2003).
16. Q. Wan, T. H. Wang, and J. C. Zhao, *Appl. Phys. Lett.* **87**, 083105 (2005).
17. Von G. U. Oertzen, R. T. Jones, and A. R. Gerson, *Phys. Chem. Miner.* **32**, 255 (2005).
18. M. Acı and M. Avcı, *Appl. Phys. A* **122**, 631 (2016).
19. X. Jia, H. Q. Zhang, Z. Wang, C. L. Jiang, Q. J. Liu, and Z. T. Liu, *Moscow Univ. Phys. Bull.* **72**, 358 (2017).

20. I. O. Alp and Y. O. Ciftci, *J. Electron. Mater.* **47**, 272 (2018).
21. R. de Alencar Rocha, W. F. da Cunha, and L. A. Ribeiro, *J. Mol. Model.* **25** (9), 290 (2019).
22. S. J. Clark, M. D. Segall, C. J. Pickard, P. J. Hasnip, M. I. Probert, K. Refson, and M. C. Payne, *Zeitschr. Kristallogr.–Cryst. Mater.* **220**, 567 (2005).
23. M. D. Segall, P. J. Lindan, M. A. Probert, C. J. Pickard, P. J. Hasnip, S. J. Clark, and M. C. Payne, *J. Phys.: Condens. Matter* **14**, 2717 (2002).
24. A. Yoshinari, K. Ishida, K. I. Murai, and T. Moriga, *Mater. Res. Bull.* **44**, 432 (2009).
25. L. Lezhong, Y. Weiqing, D. Yingchun, and Z. Xinghua, *J. Semicond.* **33**, 012002 (2012).
26. M. K. Yaakob, N. H. Hussin, M. F. M. Taib, T. I. T. Kudin, O. H. Hassan, A. M. M. Ali, and M. Z. A. Yahya, *Integr. Ferroelectr.* **155**, 15 (2014).
27. Y. Deng, O. H. Jia, X. R. Chen, and J. Zhu, *Phys. B (Amsterdam, Neth.)* **392**, 229 (2007).
28. Y. Liu, L. Fang, H. Lu, Y. Li, C. Hu, and H. Yu, *Appl. Catal. B: Environ.* **115**, 245 (2012).
29. Y. Liu, L. Fang, H. Lu, L. Liu, H. Wang, and C. Hu, *Catal. Commun.* **17**, 200 (2012).
30. W. Teng, X. Li, Q. Zhao, J. Zhao, and D. Zhang, *Appl. Catal. B: Environ.* **125**, 538 (2012).
31. X. Hong, X. Wu, Q. Zhang, M. Xiao, G. Yang, M. Qiu, and G. Han, *Appl. Surf. Sci.* **258**, 4801 (2012).
32. Y. Bi, S. Ouyang, N. Umezawa, J. Cao, and J. Ye, *J. Am. Chem. Soc.* **133**, 6490 (2011).
33. G. Botelho, J. C. Sczancoski, J. Andres, L. Gracia, and E. Longo, *J. Phys. Chem. C* **119**, 6293 (2015).
34. X. Guan and L. Guo, *ACS Catal.* **4**, 3020 (2014).
35. F. J. Zhang, F. Z. Xie, S. F. Zhu, J. Liu, J. Zhang, S. F. Mei, and W. Zhao, *Chem. Eng. J.* **228**, 435 (2013).
36. Y. Lv, K. Huang, W. Zhang, B. Yang, F. Chi, S. Ran, and X. Liu, *Ceram. Int.* **40**, 8087 (2014).
37. P. Reunchan and N. Umezawa, *J. Phys. Chem. C* **119**, 2284 (2015).
38. S. Zhang, S. Zhang, and L. Song, *Appl. Catal. B: Environ.* **152**, 129 (2014).